

CONSTRUCTION OF A 3-D P AND S MODEL OF THE CRUST AND UPPER MANTLE TO IMPROVE REGIONAL LOCATIONS IN W. CHINA, CENTRAL ASIA, AND PARTS OF THE MIDDLE EAST

Michael H. Ritzwoller, Mikhail P. Barmin, Antonio Villasenor, Anatoli L. Levshin, E. Robert Engdahl
Department of Physics, University of Colorado at Boulder

Wim Spakman, Jeannot Trampert
University of Utrecht, The Netherlands

Sponsored by Defense Threat Reduction Agency
Contract No. DTRA01-99-C-0019

ABSTRACT

Our overall goal is to assess the capabilities of three-dimensional (3-D) velocity models of the crust and upper mantle to improve the location of small seismic events within a regional monitoring environment. By "regional" we mean using data with path lengths confined to be less than about 2500 km. Our concentration is on the region bounded by latitudes 15° N to 55° N and longitudes 40° E to 100° E. We are now taking the first steps in this direction by constructing and testing a new 3-D S-model of the crust and upper mantle beneath the region of study and comparing it with the P-model of Bijwaard et al. (1998). Our S-model is a regional model of the crust and upper mantle, currently on a 2° x 2° grid, obtained by simultaneous inversion of broadband group velocity (e.g., Ritzwoller and Levshin, 1998; Ritzwoller et al., 1998) and phase velocity dispersion measurements (e.g., Trampert, and Woodhouse, 1996) constrained to fit a priori information about crustal and mantle structures. We find that most of the data used in the inversion can be well fit with a simple model of the crust and mantle that remains faithful to the a priori information. Crustal and mantle structures, with a few exceptions, demonstrate remarkable agreement with tectonic features and S-anomalies in the mantle agree favorably in both distribution and magnitude with the P-model of Bijwaard et al., (1998). In the crust, the tectonically deformed areas are typically slow (e.g., Turkey, Zagros in W. Iran, Hindu Kush in Afghanistan, Tibet, etc.) and shields and other stable regions are fast. Sedimentary basins are underlain by high velocities. The S-model between Moho and 220 km depth is transversely isotropic. The transverse isotropy is pervasive and, on average, somewhat stronger than that in PREM with the strongest anisotropy beneath tectonically deformed regions and shields. Consistent with PREM, vsh is almost everywhere faster than vsv and a low velocity zone typically arises for vsh across most of Eurasia but only rarely occurs for vsv.

Capabilities for computing Travel Time Correction Surfaces (TTCS) from 3-D models using 3-D ray tracing are now in place and we show examples TTCSs from our S-model and the P-model of Bijwaard et al. (1998). We demonstrate the relative importance of the crustal and mantle components of the TTCSs. Because crustal and mantle contributions may anticorrelate (e.g., Tibet), in order to predict regional travel time corrections accurately requires good 3-D models of both the crust and the upper mantle.

Due to different data and inversion methods, the P and S models display different and complementary strengths and weaknesses. The hybrid model that we will construct will be designed to exploit the strengths of the different data sets and inversion methods. The future combination of the P and S models will be facilitated by a new data base of P and S station corrections compiled for the region of study. The figure of merit in this hybridization will be the ability to improve the locations of Ground Truth events.

Key Words: Earth models, correction surfaces, event location, regional monitoring, path calibration

OBJECTIVE

The objective is to provide accurate P- and S-wave path calibrations rapidly and efficiently for the region of study. The method relies on the development, validation, and application of a 3-D model of the crust and upper mantle from which travel time correction surfaces (TTCS) can be computed for arbitrary body wave phases and event and station coordinates. The predicted TTCSs are intended for use within a hierarchy of information to improve path calibrations which are integral to the accurate location of small events with regional data alone. Model predictions are particularly useful in interpolating and extrapolating empirical information, in otherwise uncalibrated regions, for uncalibrated phases, and for newly installed stations.

RESEARCH ACCOMPLISHED

Introduction: The Problem

We approach model-based path calibration in three stages: (1) model construction, (2) model verification and calibration, and (3) validation and Ground Truth Event relocation. We report here only on aspects of the first stage, the construction of a model of the crust and upper mantle for much of the interior of Asia ranging from about 25° E to 120° E and 10° N to 70° N, with particular concentration on the region bounded by latitudes 15° N to 55° N and longitudes 40° E to 100° E. The second stage will comprise careful tests and the modification of the model using regional seismic data. We will also bring to bear information that is not easily applied during model construction; for example crustal velocities from individual refraction profiles. In the final stage, we will characterize the ability of the model to improve the relocation of Ground Truth Events in the region of study.

The challenge at the model construction stage is to develop a model that fits a broad class of seismic data and a priori information, particularly about the crust. We discuss the data, a priori information, and model parameterization in the next three subsections. We conclude by showing aspects of the crustal and upper mantle components of our preliminary S-model, comparing the model with the P-model of Bijwaard et al. (1998) in the upper mantle, and displaying TTCSs for the auxiliary IMS station AAK in Kyrgyzstan.

The Data

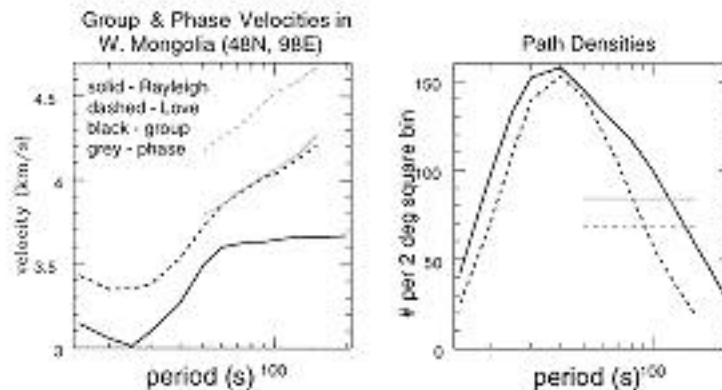


Figure 1. (LEFT) Example of the estimated group and phase velocity curves at a point in W. Mongolia. Rayleigh waves are plotted as solid lines and Love waves as dashed lines. Group velocities are black and phase velocities are grey. (RIGHT) Path densities at the same location with the same color scheme. Path densities are defined as the number of rays intersecting the 2° x 2° cell (~50,000 km²) surrounding the spatial point. Phase velocity path densities are independent of period due to the automation of the measurements.

We used the following data to construct the preliminary S-model: (1) intermediate and long period Rayleigh and Love wave group velocity maps from 15 s to 200 s period for Rayleigh waves and from 15 s

to 150 s for Love waves (e.g., Ritzwoller and Levshin, 1998; Ritzwoller et al., 1998; ciei.colorado.edu/geophysics/eurasia.dir/eurasia.html) and (2) long period Rayleigh and Love wave phase velocity maps (e.g., Trampert and Woodhouse, 1995, 1996) from 50 s to 150 s period. Figure 1 shows dispersion curves constructed from these maps at a point in W. Mongolia together with the path densities for each data type at each period. There are other notable sources of measured phase and group velocities and estimated maps, both regional and global, that we have not yet utilized (e.g., Curtis et al., 1998; Ekstrom et al., 1997; Larson and Ekstrom, 1999; Laske and Masters, 1996). We also utilize the P-wave model of Bijwaard et al. (1998) computed from groomed ISC travel times. One of the key ingredients that we are missing at the outset is data to constrain P-velocities in the crust. This is a problem that we will address in Stage 2 of the investigation. As discussed later, accurate crustal velocities are nearly as important as mantle velocities in computing TTCSs for shallow events at regional distances in the region of study.

A Priori Information

Table 1. Summary of Sources of A Priori Information

Structural Type	Source
Topography and Bathymetry	ETOP05 (NOAA/NGDC/World Data Center A)
Sedimentary Thickness & Velocities	Laske and Masters, 1997
Crustal Velocities	Mooney et al., 1998 (CRUST5.1)
Moho	Kunin et al., 1987 (IPE) Seeber et al., 1997 Laske and Masters, 1999 Mooney et al., 1998 (CRUST5.1)
Upper Mantle Velocities	Masters et al., 1996 (S16B30) Bijwaard et al., 1998
Lower Mantle Velocities	Masters et al., 1996 (S16B30)

The inverse problem is characterized by strong trade-offs between crustal and mantle structures and among various crustal structures. These trade-offs are not easily resolved by adding more data of the types described above, although the use of short period Rayleigh and Love wave group velocities does help in this direction. Rather it is necessary to constrain the space of models by applying a priori information about the crust, in particular, in the inversion. Because surface wave sensitivity kernels depend on the unknown structure, the inversion is non-linear and the inferred model depends on the starting model. Thus, an accurate starting model and the application of constraints on allowed perturbations during inversion are necessary ingredients to ensure that a high quality model will emerge from the inversion.

Fortuitously, efforts by several researchers have yielded information about crustal and upper mantle structures across parts of Eurasia in an organized form. We have used information from the sources listed in Table 1. Our input model is based on topography and bathymetry from ETOP05, sedimentary thickness and velocities from the 1° x 1° compilation of Laske and Masters (1997), crustal velocities below the sediments from the 5° x 5° model CRUST5.1 of Mooney et al. (1998), Moho topography from the sources listed in Table 1 with a specified precedence ordering (Laske and Masters, 1999; Kunin et al., 1987; Mooney et al., 1998), and upper mantle velocities from the isotropic spherical harmonic degree 16 model S16B30 of Masters et al. (1996). We are currently investigating conversion of P to S in order to use a smoothed version of the model of Bijwaard et al. (1998) as a starting mantle model. These models have resolutions ranging from ~10² km to >10³ km and there are variable accuracies within and between the models. Constraints on the structural perturbations allowed during inversion must attempt to account for these differences.

Model Parameterization and Inversion

We have attempted to find a simple, albeit entirely ad hoc, parameterization of the model that will allow us to fit the observed data while remaining faithful to the a priori information discussed in the previous subsection. At each spatial point the group and phase velocity data are inverted iteratively by perturbing the variables displayed

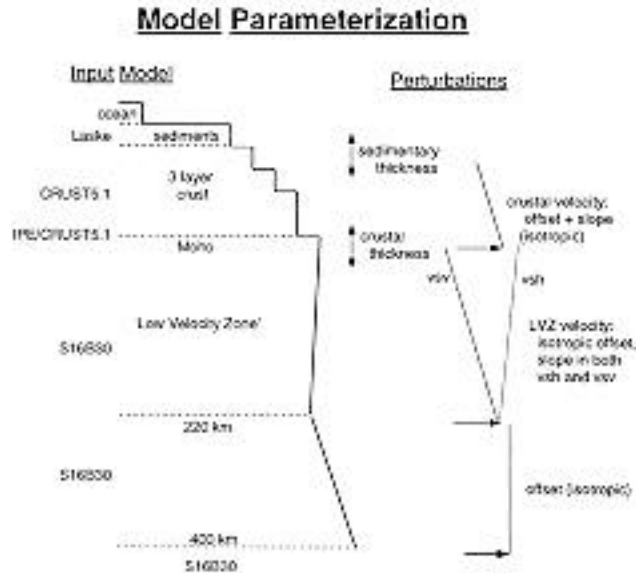


Figure 2. Schematic representation of the parameterization of the model. The left column depicts the form of the isotropic input model which is divided into the following layers: an ocean, two-layer sediments, three-layer crust, the Low Velocity Zone extending between the Moho and 220 km depth, and a layer between 220 km and 400 km depth. Surface topography, ocean bottom bathymetry, sediment thicknesses and velocities, crustal velocities, Moho depths, and mantle shear velocities are taken from sources described above. The right column depicts the estimated perturbations: depth shifts in the sediment bottom and Moho, offsets in the average shear velocity of the crust and the mantle from Moho - 220 km and 220 km - 400 km, and changes in the vertical gradient of shear velocity in the crust and from Moho - 220 km.

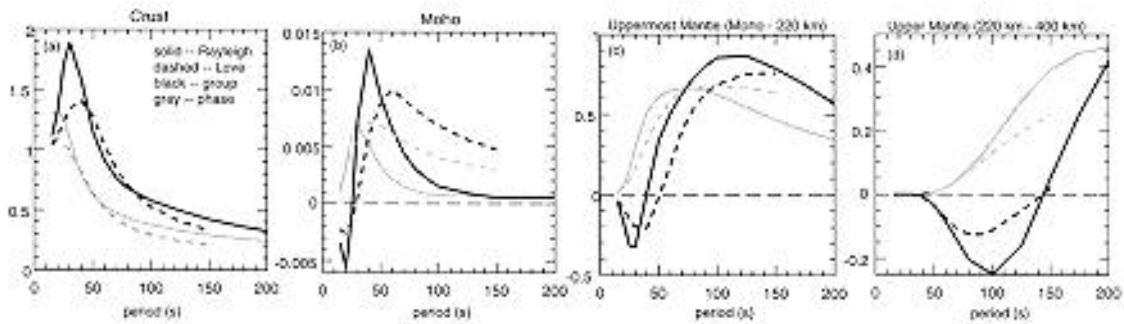


Figure 3. Partial derivatives of Rayleigh and Love wave group and phase velocities with respect to four of the structures in the current parameterization of our S-wave model: (a) constant crustal vs perturbation, (b) topographic perturbation to Moho, (c) constant mantle isotropic vs perturbation between 220 km and 220 km, and (d) constant mantle vs perturbation between 220 km and 400 km. Solid lines are Rayleigh waves, dashed lines are Love waves, black is group velocity, and grey is phase velocity. In general, phase velocities sample deeper than group velocities and Rayleigh deeper than Love at each period. Thus, partial derivatives for phase velocities peak at shorter periods than group velocities and Rayleigh at shorter periods than Love. The group velocity partials change sign.

schematically in Figure 2. We recompute the partial derivatives on each iteration and iterate until convergence, usually 5 - 8 iterations. Figure 3 displays examples of partial derivatives for a number of model variables computed in W. Mongolia. This figure demonstrates the importance of the long period phase velocities in improving the sensitivity to shear velocities below 200 km and the importance of the short and intermediate period group velocities in constraining crustal structures. Data weights based on path density and residuals are applied during inversion and structural tolerances are chosen automatically depending on the data distribution. For example, if short period data are missing crustal tolerances are tightened and if long period information is missing mantle tolerances are tightened. For the model displayed in the next subsection, we have allowed perturbations to the input sedimentary thickness and Moho depth of no more than ± 5 km but have allowed much more generous perturbations to crustal and mantle velocities which we believe are more poorly known in the input model.

An important observation is that we are not able to fit both the long period Rayleigh and Love wave data simultaneously without a transversely isotropic uppermost mantle. This is the reason we have introduced the anisotropy between Moho and 220 km depth. In addition, we found it necessary to perturb not only the average velocity of the crust, but also to allow a change in the vertical gradient of the crustal shear velocities.

If the data warrant, the resulting parameterization contains eight variables, which is beyond the capacity of current data to estimate simultaneously. We damp the inversion on each iteration and allow the algorithm to choose the subset of variables to perturb and to resolve the trade-offs given the constraints we place on the inversion.

Figure 4 presents an example of the results of the inversion in Western Mongolia. The group and phase velocity data can be well fit simultaneously across most of Eurasia. Exceptions have motivated our parameterization. There remain problems, however, with discrepancies between the Rayleigh and Love wave maps and between the group and phase velocity maps that arise due to different intrinsic resolutions between the different data types. The inversion algorithm recognizes these discrepancies, chooses a subset of the data to fit, and tightens tolerances when this problem arises.

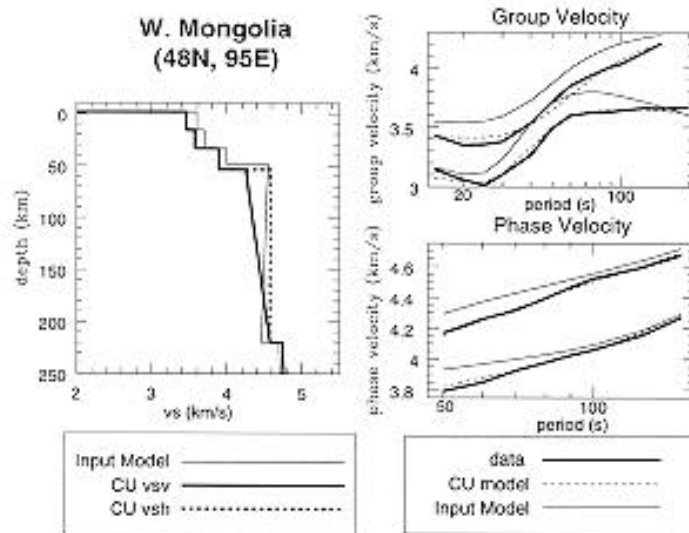


Figure 4. (LEFT) Estimates and input shear velocity profiles under the specified point. The input profile is the thin solid line and is isotropic, as defined above. The estimated profile is the thick solid and dashed lines and is transversely isotropic between Moho and 220 km depth and isotropic elsewhere. Typically $v_{sh} > v_{sv}$ and a low velocity zone is evidenced between Moho and 220 km in v_{sh} but not in v_{sv} . (RIGHT) Comparison between observed group and phase velocities and predictions from the input and estimated models. The data are the thick solid lines whereas the thin solid lines and the dashed lines are the prediction from the input model and the estimated model, respectively.

Our S-model is currently produced on a 2° x 2° degree grid, but we will soon move to 1° x 1°.

Preliminary Shear Velocity Model

Figure 5 presents aspects of the crustal model across the studied region. The sedimentary thickness and Moho depths have been constrained to lie within 5 km of the input model and thus contain little new information. The crustal velocities, however, represent large perturbations from the input model. The upper crust, in particular, displays very strong tectonic correlation. The tectonically deformed areas are typically slow (e.g., Turkey, Zagros in W. Iran, Hindu Kush in Afghanistan, Tibet, etc.) and shields and other stable regions are fast. Sedimentary basins are underlain by high velocities. Clearly, there remain problems; e.g., we have lost the Moho depression under the Zagros and it remains an open question how to estimate crustal P from the crustal S-model. These are questions for on-going research.

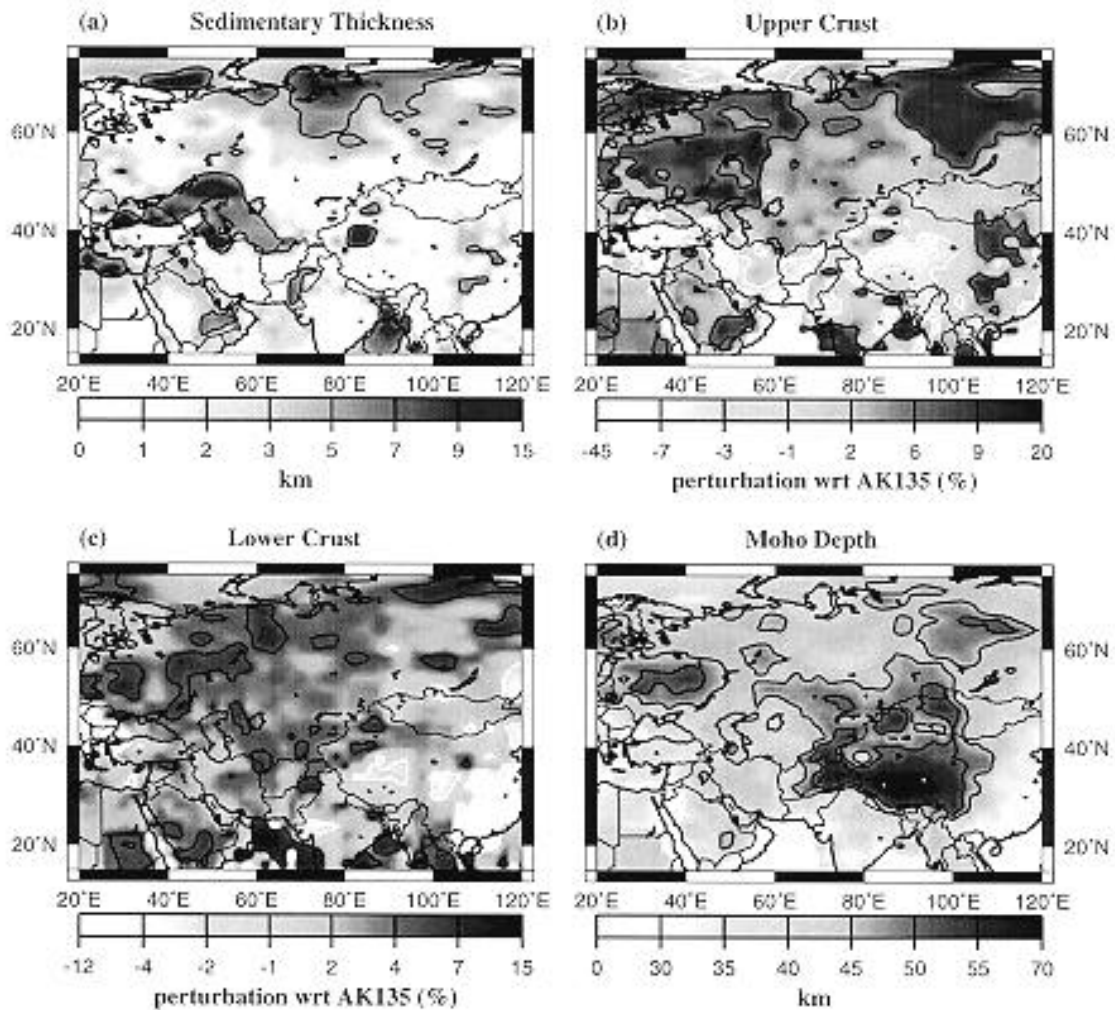


Figure 5. The estimated model of the crust. (a) Sedimentary thickness in km. The 5 km contour is displayed. (b) Upper crustal shear velocity as percent perturbation relative to AK135 (3.46 km/s). The +5% and -3% contours are displayed. (c) Lower crustal shear velocities relative to AK135 (3.85 km/s). The +5% and -2% contours are displayed. (d) Moho depth below the geoid in km. The 45 km and 50 km contours are displayed.

The upper mantle velocity variations demonstrate somewhat larger scale features than the crustal anomalies because they arise to fit the longer wavelength intermediate and longer period surface wave data. The model between the Moho and 220 km depth is transversely isotropic. The transverse isotropy is pervasive and, on average, somewhat stronger than that in PREM with the strongest anisotropy beneath tectonically deformed regions and shields. As evidenced in Figure 4 and consistent with PREM, vsh is almost everywhere faster than vsv. Also consistent with PREM, a low velocity zone typically arises for vsh across most of Eurasia but only rarely occurs for vsv.

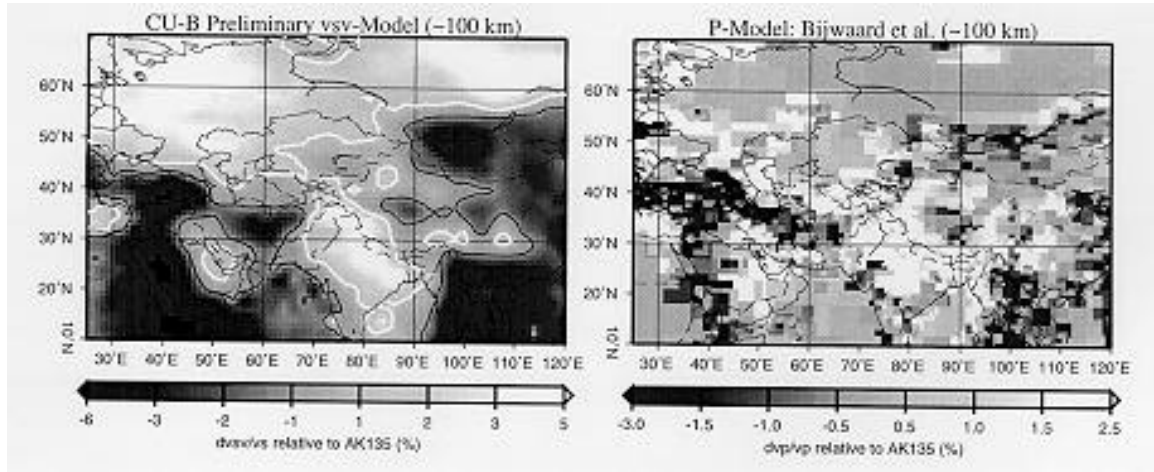


Figure 6. Comparison at about 100 km depth between our estimated S-model (vsv) and the P-model of Bijwaard et al. (1998). The S-model is presented as percent perturbation to S-velocity from AK135 (4.5 km/s) and the P-model is relative to P-velocity from AK135 (8.05 km/s). In the left plot, the +/-1% contours are shown as white and black lines, respectively.

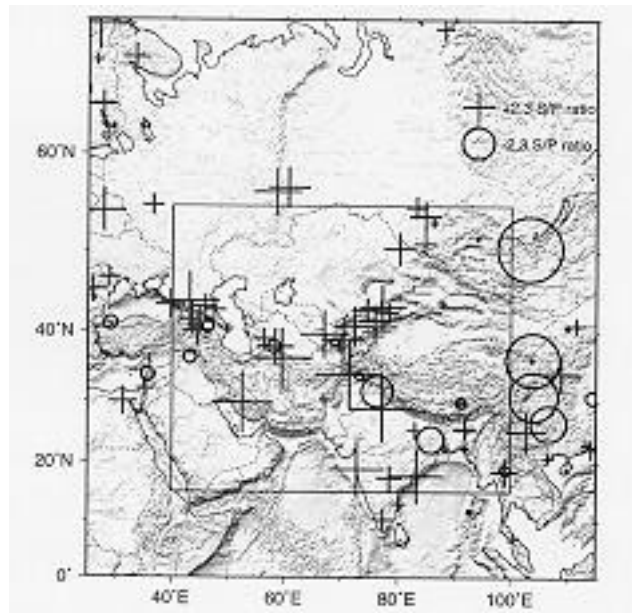


Figure 7. S/P ratios of station residual medians. Pluses correspond to correlated P and S station corrections and minuses to anticorrelated station corrections. Most stations show a positive correlation and the slope of the P- correction to S-correction graph is 2.3. Anticorrelations cluster, however, and are probably physically meaningful. The cause of the anticorrelations is not yet clear.

Figure 6 presents a comparison between our preliminary S-model at 100 km depth in the upper mantle and the P-model of Bijwaard et al. (1998) at approximately the same depth. It is important to recognize that at this depth, the P-model is poorly resolved over large areas characterized by little seismicity and few historical stations (e.g., Russian Platform, Siberian shield, Kazakh Platform, Egypt/Sudan, Arabian Sea, Bay of Bengal, S. China Sea, and other areas). These areas are indicated by larger block sizes in the P-model, but are difficult to see in Figure 6. In the regions with adequate coverage by both P-waves and surface waves the agreement is very good, however.

These observations encourage interconversion of the P variations to S variations and conversely in order to take advantage of the relative strengths and weaknesses of the two models. The P-model displays better lateral resolution than the S-model, but the S-model has more homogeneous coverage. In addition, we have an S-model for the crust but no P-model, but the P-model improves with depth below 200 km and the S-model loses its resolution rapidly below this depth. Figure 7 shows P/S ratios from station corrections computed from the groomed ISC data base across the region of study. Although there are occasional anticorrelations, most stations demonstrate correlated P and S station corrections in both amplitude and azimuthal distribution with a slope of about 2.3.

Preliminary Travel Time Correction Surfaces (TCCS)

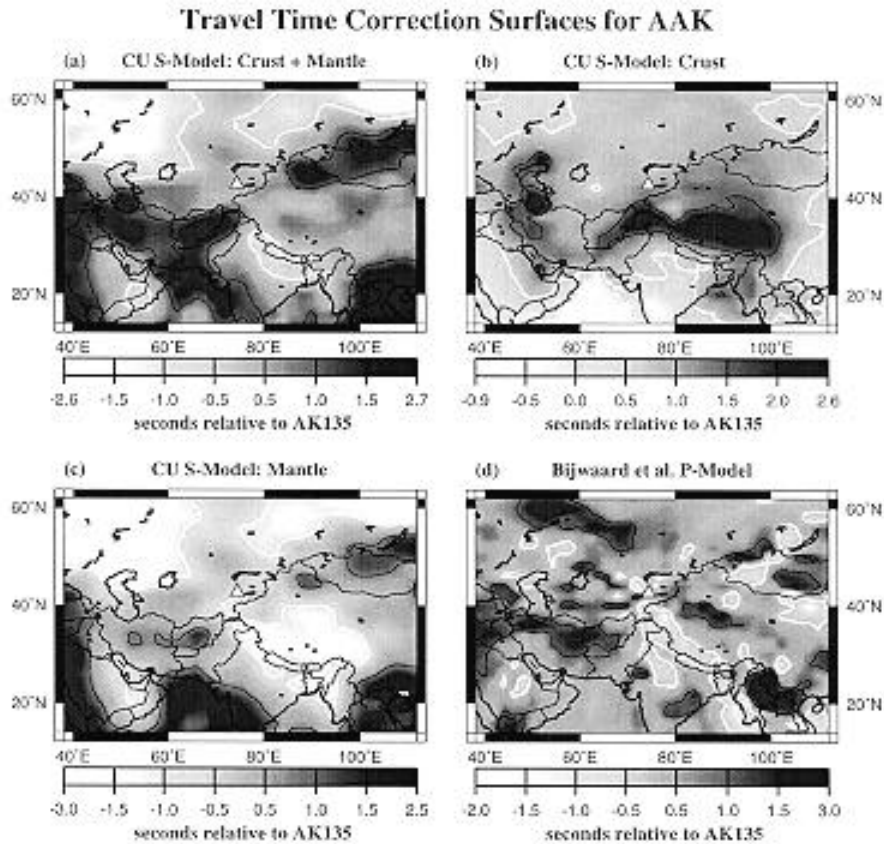


Figure 8. Predicted travel time correction surfaces for the station AAK for a surface event. The value on the map is the specified first arriving body wave travel time relative to the prediction from the laterally homogeneous model AK135. (a) S-wave correction surface for our S-model. The -0.5 s and 1.0 s contours are shown with white and black lines, respectively. (b) S-wave correction surface for the crustal component of our S-model. The 0.5 s and 1.5 s contours are displayed. (c) S-wave correction surface for the mantle part of our S-model. The -0.5 and 0.75 s contours are shown. (d) P-wave correction surface for the P-model of Bijwaard et al. (1998). The -0.25 s and 1.0 s contours are shown.

The computation of a TTCS for a given station from a 3-D model is straightforward. A fictitious event is placed at each geographical position at a given depth. Here we use the geoid as the hypocentral depth in dry continental areas and the solid surface in wet continental and oceanic areas. We trace a 3-D ray from the hypocenter to the station (placed at the geoid here) for each fictitious event using the 3-D ray tracing code described by Pulliam and Snieder (1998). The fictitious events are moved systematically around the region of study. We reference each 3-D travel time to the travel time predicted from the laterally homogeneous model AK135 (Kennett et al., 1995) and define a travel time correction as the difference between the travel time through the 3-D model and the AK135 time. Thus, positive residuals are slow and negative residuals are fast in the usual way.

Figure 8 shows a set of such TTCSs for the auxiliary IMS station AAK. Figures 8a - 8c are computed using the preliminary S-model described above. Several observations are worth noting. First, the travel time corrections are simply related to the features of the model displayed in Figures 5 and 6. On average, tectonically deformed regions produce slow travel times and shields and plate boundaries characterized by thickened lithosphere are fast. Comparison of Figures 8b and 8c reveals that in these regions the crustal and mantle contributions to the corrections correlate and add constructively. Indeed, for shallow events the crustal and mantle contributions are of nearly the same expected magnitude and in these regions the crustal contribution only affects the total travel time correction by changing the amplitude of the prediction from the mantle model. Crustal and mantle contributions frequently anticorrelate, however, as exemplified by the Tibet region. Thus, to predict regional travel time corrections accurately requires both good crustal and mantle models.

Figure 8d, computed similarly for the P-model of Bijwaard et al. (1998), compares most favorably with the mantle part of our S-model. (This comparison, as in Figure 6, must be informed by knowledge of the regions poorly constrained by the P-model; e.g., much of N. Asia, Arabian Sea, Bay of Bengal.) This is expected due to the lack of a crustal component in this P-model. By combining the S-model and the P-model to take advantage of the strengths of each, we plan to produce a hybrid model that will improve the TTCSs for both S and P. The figure of merit in this hybridization is the ability to improve the locations of Ground Truth events.

CONCLUSIONS AND RECOMMENDATIONS

We present here some of the preliminary results that have emerged concerning the new S-model across the studied region. The potential for the use of this and related models for path calibration is encouraging. Most of the data used in the inversion can be well fit with a simple model of the crust and mantle that remains faithful to a priori information. Crustal and mantle structures, with a few exceptions, demonstrate remarkable agreement with tectonic features and S-anomalies in the mantle agree favorably in both distribution and magnitude with a recent P-model of the mantle (Bijwaard et al., 1998). Capabilities are now in place to compute Travel Time Correction Surfaces (TTCS) from this or other models of the region of study. Problems remain that we are continuing to address. Perhaps most significantly, we possess constraints only on crustal shear velocities and must convert the crustal S-model to a P-model. Inspection of P and S station corrections and comparison between the S-model and the P-model of Bijwaard et al. (1998), however, encourage us to investigate the interconversion between the P and S models to take advantage of their complementary strengths and weaknesses.

We anticipate completion of the combined P- and S-model in several months. The verification and further development of this model with local and regional seismic data is an important next step in this research. All developments of the model occur within the framework of improving regional location capabilities within the area of study.

REFERENCES

- Bijwaard, H., W. Spakman, and E.R. Engdahl, Closing the gap between regional and global travel time tomography, *J. Geophys. Res.*, 103, 30055 - 30078, 1998.
- Curtis, A., J. Trampert, R. Snieder, and B. Dost, Eurasian fundamental mode surface wave phase velocities and their relationship with tectonic structures, *J. Geophys. Res.*, 103, 26919 - 26947, 1998.
- Ekstrom, G., J. Tromp. And E.W.F. Larson, Measurements and global models of surface wave propagation, *J. Geophys. Res.*, 102, 8137 - 8158, 1997.
- Kennett, B.L.N., E.R. Engdahl, and R. Buland, Constraints on seismic velocities in the Earth from travel-times, *Geophys. J. Int.*, 122, 108 - 124, 1995.
- Kunin, N.Y., et al., Eurasian Moho relief map, *Inst. of Phys. of the Earth, Acad. of Sci., Minist. of Geol. of the Russ. Fed., Moscow*, 1987.
- Laske, G. and G. Masters, Constraints on global phase velocity maps from long-period polarization data, *J. Geophys. Res.*, 101, 16059 - 16075, 1996.
- Laske, G. and G. Masters, A global digital map of sediment thickness, *EOS Trans. AGU*, 78, F483, 1997. (mahi.ucsd.edu/Gabi/sediment.html)
- Laske, G. and G. Masters, A global digital map of crustal thickness, unpublished, 1999.
- Larson, E.W.F. and G. Ekstrom, Global models of surface wave group velocity, submitted to *Pageophys.*, 1999. Masters, G., S. Johnson, G. Laske, and H. Bolton, A shear-velocity model of the mantle, *Phil. Trans. R. Soc. London, Ser. A.*, 354, 1385 - 1411, 1996.
- Mooney, W.D., G. Laske, and G. Masters, CRUST5. I: A global crustal model at 5' x 5', *J. Geophys. Res.*, 103, 727 - 747, 1998. (mahi.ucsd.edu/Gabi/crust.html)
- Pulliam, J and R. Snieder, Ray perturbation theory, dynamic ray tracing, and the determination of Fresnel zones, *Geophys. J. Int.*, 135, 463 - 469, 1998.
- Ritzwoller, M.H. and A.L. Levshin, Eurasian surface wave tomography: Group velocities, *J. Geophys. Res.*, 103, 4839 - 4878, 1998.
- Ritzwoller, M.H., A.L. Levshin, L.I. Ratnikova, and A.A. Egorkin, Intermediate period group velocity maps across Central Asia, western China, and parts of the Middle East, *Geophys. J. Int.*, 134, 315-328, 1998. Seeber, D., M. Vallve, E.A. Sandvol, D.N. Steer, and M. Barazangi, Middle East tectonics; applications of geographic information systems (GIS), *GSA Today*, 7, 1 - 6, 1997.
- Trampert, J. and J.H. Woodhouse, Global phase velocity maps of Love and Rayleigh waves between 40 s and 150 s period, *Geophys. J. Int.*, 122, 675 - 690, 1995.
- Trampert, J. and J.H. Woodhouse, High resolution global phase velocity distributions, *Geophys. Res. Let.*, 23(1), 21-24, 1996.